PHYSICAL REVIEW B VOLUME 45, NUMBER 14 1 APRIL 1992-II

In situ x-ray studies of rapid crystallization of amorphous $NiZr_2$

S. Brauer, J. O. Ström-Olsen, M. Sutton, Y. S. Yang, and A. Zaluska
Centre for the Physics of Materials and Department of Physics, McGill University,
Rutherford Building, 3600 University Street, Montréal, Québec, Canada H3A 2T8

G. B. Stephenson
IBM Research Division, Thomas J. Watson Research Center, Yorktown Heights, New York 10598

U. Köster
Department of Chemical Engineering, University Dortmund, D-4600 Dortmund 50, Germany

(Received 11 April 1991; revised manuscript received 7 October 1991)

We have studied the crystallization of amorphous $NiZr_2$, using time-resolved x-ray scattering, for crystallization times varying from several minutes to tens of milliseconds. At relatively low temperatures, where the kinetics of transformation are slow, crystallization of the equilibrium $NiZr_2$ phase occurs by time-dependent nucleation and growth. As the transformation temperature is increased, an ever greater fraction of a transient metastable crystal phase is formed, *before* the equilibrium phase is reached. We believe that the transient phase is in fact a precursor to the formation of the equilibrium phase at all temperatures. By rapidly quenching samples containing this transient phase, we have, by x-ray and electron diffraction, identified the crystal structure as belonging to the space group O_h^7, with a lattice parameter of 12.61 ± 0.01 Å. The transient phase is believed to be formed because it is structurally closer to the amorphous than the equilibrium phase, thereby requiring less atomic rearrangements to form. By considering the formation of the O_h^7 structure in similar (transition-metal)-Zr_2 alloys, we deduce that the stability of the transient phase is closely related to the filling of the electronic *d* band.

I. INTRODUCTION

A rich mixture of nonequilibrium phenomena occur as amorphous materials transform to the crystalline state. In the simplest picture, the amorphous material is in a thermally arrested mestastable state, which undergoes a first-order phase transformation to a crystalline state, by nucleation and growth. Measurements of the kinetics of the process provide a test of nucleation and growth models in the solid state.

Time-resolved x-ray scattering provides an ideal tool for investigating these irreversible processes. Such *in situ* studies provide detailed structural information about the crystallizing material throughout the transformation. Moreover, advances in x-ray flux and detection in concert with techniques for rapidly changing and controlling the state of the system under study, permit crystallization measurements on time scales that are orders of magnitude smaller than those of conventional techniques.

The crystallization rate is a maximum at a temperature somewhat below the freezing point. This maximum is determined by a tradeoff between the decreasing free-energy difference, which drives the transformation, and the increasing atomic mobility as the sample temperature is increased. Most structural studies of crystallization in amorphous metals have only been done at temperatures well below the maximum rate. (Reference 1 is an exception.) We have previously reported results of crystallization studies in the model metallic glass $Ni_{33.3}Zr_{66.7}$, hereafter written simply as NiZ_2, wherein an unexpected transient structure was observed during the most rapid transformations.[2] We report here on even faster crystallization experiments in the $NiZr_2$ system, made possible through new high-speed temperature control techniques.[3] The amount of the transient structure formed increases with the rate of transformation and sufficient quantities of the phase have been formed to identify it, using both x-ray and electron diffraction, with an O_h^7 ($Fd3m$) structure in nominally pure $NiZr_2$ The kinetics of formation and decomposition of the transient phase, and the effects of the transient on the crystallization of the conventional phase are presented.

II. EXPERIMENTAL METHODS

A. Time-resolved x-ray scattering

Detailed descriptions of our experimental setup have been published previously.[3,4] In a typical experiment, crystallization is brought about by abruptly heating a specimen from room temperature to a prescribed transformation temperature. Simultaneously, x-ray-diffraction patterns are repeatedly acquired as the system evolves toward thermodynamic equilibrium at the new temperature.

The experiments are conducted at the National Synchrotron Light Source at Brookhaven National Laboratory, with the IBM/MIT beamline X-20C. This beamline is equipped with a platinum-coated silicon 1:1 focusing mirror, which collects 4 mrad of dipole-bending-magnet synchrotron radiation and focuses it to a 1 mm×1 mm spot at the sample position, 22 m from the source. A wide-bandpass artificial-multilayer monochromator gives an energy resolution of 1% at the energy used (6 keV). The q-space resolution is a convolution of the energy resolution with the geometrical resolution resulting from the finite beam size on the sample. It has been both measured and calculated to be $\delta q/q = 0.025 \pm 0.002$.

At a typical synchrotron ring current of 100 mA, the beamline provides an incident intensity of 10^{13} photons per second. Diffraction profiles are measured in reflection by a linear position-sensitive detector consisting of a photodiode array with 1024 pixels spanning 25 mm (Fig. 1).[5] The pixels can be electronically grouped to improve time resolution at the expense of spatial resolution. In the 64-pixel configuration selected for these experiments, diffraction patterns could be collected as fast as every 3 ms. The detector was placed 78 mm from the scattering volume and centered at a scattering angle of $2\theta = 50°$. The absorption length of 6-keV xrays in $NiZr_2$ is 6 μm so that half of the scattering comes from the top 1 μm of the specimen.

The time-resolved scattering data yields detailed structural information about the transforming material, such as lattice parameters, mean grain size (for grains smaller than our resolution limit), evidence of faulting or disorder from the peak shapes and intensities and, most importantly for these studies, which phases are present and to what extent. For $NiZr_2$, when the kinetics are slow enough that individual diffraction patterns are collected over 1 s or more, counting statistics are sufficiently good that crystalline volume fractions as small as 0.1% can be measured.[6]

B. Temperature measurement and control

For the transformation to be effectively isothermal (which greatly simplifies any quantitative analysis of the results), the transient in the temperature step must be much shorter than the phase-transition time. To take full advantage of the available x-ray-diffraction time resolution, it was necessary to develop techniques to change sample temperature by hundreds of degrees of milliseconds, in a uniform and controlled manner. In general, temperature control on short time scales requires high heating and cooling power, and samples of small heat capacity. The characteristic time to achieve thermal equilibrium is then short, so that the temperature can be abruptly changed and thermal disturbances, such as variations in sample properties, can be quickly and efficiently compensated.

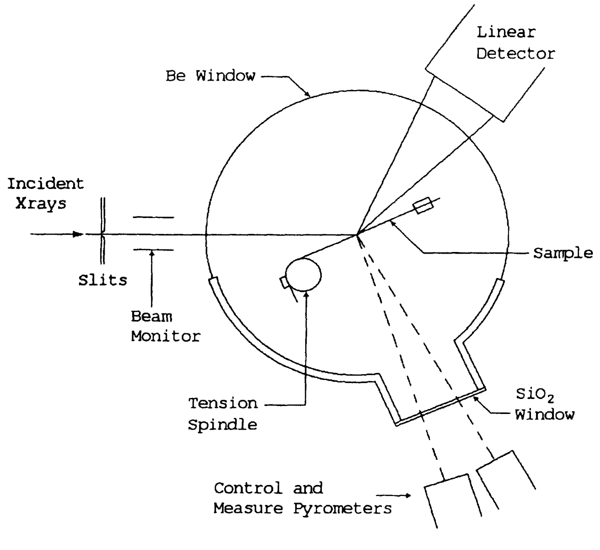

FIG. 1. Schematic of the experimental setup used in time-resolved x-ray-scattering experiments.

Melt spun ribbon samples, typically 35 mm long, 1 mm wide, and 25 μm thick are ideal for our studies, since they provide small thermal mass yet appreciable surface area for x-ray scattering and for cooling. When suspended between water-cooled posts in a helium gas atmosphere, the samples can be heated to temperatures in the range 500–1100 K by passing direct current along their length. In the steady state, Joule heat generated throughout the volume of the sample is removed from the surface by radiation and heat exchange with the gas. For thin ribbons of uniform cross section, the geometry produces a large central region of uniform temperature, because both conduction along the ribbon and thermal gradients through the ribbon thickness are negligible. Full advantage is taken of the small thermal mass because only the sample and a small volume of the surrounding gas are heated. Furthermore, the heating power is limited only by the available current. If the heating power is turned off, cooling rates of more than 10^3 Ks^{-1} are typical so that phases can be rapidly quenched in at any time during the transformation for subsequent microstructural measurements.

The sample chamber was pumped to $\approx 10^{-7}$ Torr before backfilling with 99.9999% purity He. Because the samples showed no signs of surface oxidation after the crystallization, we believe oxygen contamination was prevented.

Temperature is measured with an infrared pyrometer because any contact probe would reduce thermal time response and degrade temperature uniformity. Absolute temperature calibration of ± 5 K is possible by comparing the rates of slow transformations with scanning-calorimetry results.

For these irreversible phase transformations, it is crucial to avoid overshoot in the temperature step, since the transformation kinetics vary exponentially with temperature. In $NiZr_2$, near 640 K, the time to crystallize 50 vol% is halved with each 8 K increase in temperature. Temperature overshoot would thus yield misleading results for the transformation kinetics. A high-power proportional temperature control loop[3] provides an abrupt, nonovershooting step to the transformation temperature. The controller can be used with either a 25-μs response pyrometer for subminute crystallizations runs, or with a 10-ms response commercial pyrometer[7] for longer runs where a slower temperature rise is acceptable and enhanced stability is required over several minutes. When the fast pyrometer is used, the system is capable of increasing the sample temperature at rates in excess of 10^6 Ks^{-1}, without overshoot.

The temperature controller also compensates for the $\approx 20\%$ decrease in sample resistance upon crystallization. Because the controller is proportional with a finite gain, there is a small offset between the set point and the actual temperature. Since the offset changes slightly with load, ballast resistance is placed in series with the sample. If the ballast resistance is equal to the average resistance of that portion of the sample that transforms, the change in power to the sample is minimized.

The two pyrometer readings and the sample voltage and current can be sampled from 1 to 10 times as often as diffraction profiles are acquired. The power input to the specimen and the overall resistance are thus obtained as a function of time. Because of the temperature profile along the specimen, only about two-thirds of the sample crystallizes, so the resistance change is not exactly proportional to the resistivity change.

We note that the present limit to the isothermal crystallization rate is determined by the dissipation of latent heat, which disrupts the temperature uniformity. The limitation can be partly overcome by developing techniques for analyzing nonisothermal crystallization.[1]

C. The $NiZr_2$ system

Ni_xZr_{1-x} can be made amorphous over a large composition range ($x=0.2$ to 0.7) by melt spinning.[8] The composition chosen for this study ($x=\frac{1}{3}$) corresponds to the congruently melting compound $NiZr_2$ on the equilibrium phase diagram, which has a body-centered tetragonal (bct) crystal structure D_{4h}^{18} ($I4/mcm$) with $a=6.48$ Å and $c=5.24$ Å.[9] Amorphous $NiZr_2$ is therefore expected to crystallize, with only local structural changes and no long-range compositional segregation, into single-phase crystalline bct $NiZr_2$. Calorimetry studies of the crystallization show a single well-defined exothermic peak at this composition. The polymorphic crystallization was therefore expected to provide a simple, model system in which to study the kinetics of crystallization.

Samples were prepared by melting together stoichiometric proportions of Zr (nominally 99.95% pure) and Ni (99.999%) in a tungsten arc furnace under a titanium gettered argon atmosphere. The melting process was repeated several times to ensure homogeneity. Melt spinning was conducted in 35 kPa helium atmosphere with high-purity argon gas used to eject the molten alloy from a quartz crucible onto a copper wheel of tangential velocity 60 m/s. X-ray diffraction and differential scanning calorimetry were used to verify that the samples were amorphous and of the correct composition.

III. RESULTS

A. *In situ* data

Figure 2 shows a sequence of x-ray-scattering patterns from $NiZr_2$ crystallizing at 642 K, a relatively low crystallization temperature resulting in slow transformation kinetics. The total time for the transformation was about 10 min. The initial pattern is the broad first amorphous scattering peak. During the transformation, Bragg peaks from the crystalline bct $NiZr_2$ grow at the expense of the amorphous background. The widths of the diffraction peaks of the crystal phase do not change with time. This indicates that the average crystallite size is always appreciably larger than our resolution limit (100±8 Å at the strongest peak) for observable crystal volume fractions. Furthermore, no evidence for a change in shape of the amorphous peak is seen.

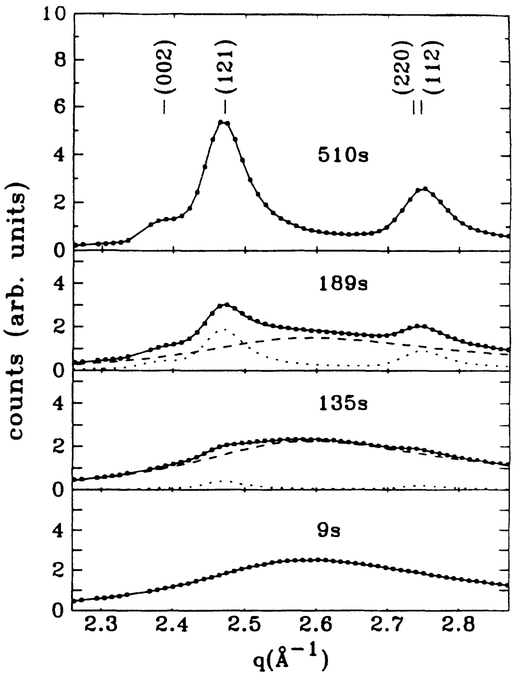

FIG. 2. Crystallization of $NiZr_2$ at 642 K. Squares represent the measured x-ray scattering and the lines through them are the results of a fit by Eq. (1). At each time, the contribution of amorphous scattering is shown as a dashed line and the bct contribution is the dotted line. The times selected are those for total crystal volume fractions of 0%, 25%, 50%, and 100%. The time per diffraction pattern is 1.5 s.

In order to determine the crystalline volume fraction as a function of time, the data of Fig. 2 was first fit with the assumption that each scattering pattern could be described as a linear combination of amorphous scattering, $I_A(q)$ and bct crystalline scattering, $I_{bct}(q)$. Explicitly, the scattering intensity used is

$$I(q,t)=[1-X(t)]I_A(q)+X(t)I_{bct}(q) , \quad (1)$$

where $X(t)$ is the volume fraction of bct crystallites. The assumption is reasonable, since the scattering intensity of each phase is proportional to the volume of material giving rise to that scattering if the scattering pattern of each phase does not change with time. The main advantage of the fitting procedure is that it determines both the loss of amorphous phase and the gain in bct phase. Furthermore, by looking for systematic variations in the quality of the fits, we can test the validity of the linear combination assumption. Whenever possible, $I_A(q)$ and $I_{bct}(q)$ were the measured scattering patterns at the initial and final times, respectively. However, $I_A(q)$ was in some cases obtained from a prefit to the initial scattering pattern using a Gaussian curve on a sloped background, and I_{bct} from a prefit to the final pattern using Gaussian-plus-Lorentzian peaks, constrained by the bct lattice parameters. For faster data, prefitting has the advantage of averaging intensity fluctuations arising from limited counting statistics. Details of the prefitting procedure are given in the Appendix. Although the fits as shown in Fig. 2 look good, there are in fact small systematic discrepancies between the data and the fit for intermediate scattering patterns.[2] This effect is explained below.

Figure 3 shows the crystallization at a higher temperature (757 K) and thus a faster rate. Even without detailed analysis, a difference between the scattering profiles at the two temperatures can be seen. At 757 K, the intermediate profiles cannot be explained as a linear combination of $I_A(q)$ and $I_{\text{bct}}(q)$. Rather, the data shows evidence of scattering peaks from a transient phase. The amount of the transient phase scattering increases with higher crystallization rates, and at the highest rates, the sample momentarily becomes almost 100% transient phase. Because of our high cooling power, it was possible to rapidly quench samples of the maximum volume fraction transient phase to room temperature, where the mobility is low enough that the structure no longer evolves in time. Electron microscopy and Cu K_α x-ray diffraction were used to identify the transient phase as O_h^7 $(Fd3m)$, a face-centered-cubic (fcc) structure, with a lattice parameter of 12.61±0.01 Å.

To deduce volume fractions of each phase from the time-resolved x-ray data, the model of Eq. (1) was modified to include scattering from the face-centered-cubic phase, $I_{\text{fcc}}(q)$. Specifically,

$$I(q,t)=[1-X(t)-Y(t)]I_A(q)+X(t)I_{\text{bct}}(q)+Y(t)I_{\text{fcc}}(q)\ , \tag{2}$$

where $Y(t)$ is the fcc volume fraction. $I_{\text{fcc}}(q)$ is the sum of Gaussian-plus-Lorentzian peaks at positions dictated by the fcc structure. For each temperature, the widths and relative intensities of these peaks were established from a fit to the pattern with the strongest fcc scattering. Only a very slight sharpening of the fcc peaks was observed during the fastest crystallization runs, and this could be ignored with little consequent error to volume fraction. The maximum volume fraction of fcc was estimated by fitting the same pattern with the model of Eq. (2), varying the overall scale of $I_{\text{fcc}}(q)$ so that $X+Y=1$.

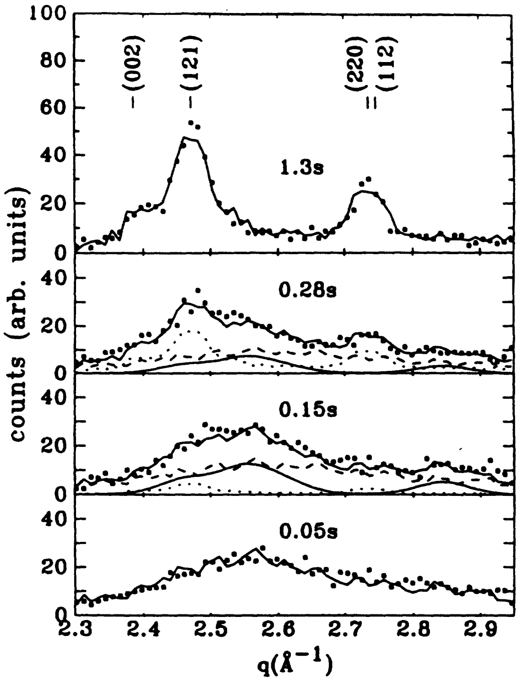

FIG. 3. Crystallization of $NiZr_2$ at 757 K. Squares represent the measured x-ray scattering and the lines through them are the results of a fit by Eq. (2). At each time, the contribution of amorphous scattering is shown as a dashed line, the bct contribution is the dotted line and the fcc contribution is the smooth solid line. The time per diffraction pattern is 0.005 s.

Figure 4 shows the sample temperature and resistance, and volume fractions of each phase as functions of time at a few different temperatures. Note that isothermal conditions are reached with no overshoot, well before there is any evidence of crystallization, in all but the fastest data set. In each case, the volume fraction of fcc crystallites initially increases in concert with the diminishing amorphous volume, reaches a maximum, and then decreases as the bct volume fraction grows to 100%. Even though the fcc contribution to the scattering is small at lower temperatures, it must be included in order for the decrease in amorphous volume fraction to be matched by the corresponding increase in crystalline volume fraction. In all our *in situ* data, the fcc phase always appears *before* the bct, implying that it is a precursor to the bct crystallization.[2]

Another striking feature shown in Fig. 4 is the initial increase in resistance seen at higher temperatures prior to the expected decrease due to bct crystallization. The resistance increase tracks the volume fraction of the fcc phase. The enhanced resistivity of the O_h^7 structure has been reported in related systems.[8,10–13] In $FeZr_2$, where the fcc phase is stable enough for grains to coarsen upon annealing, Altounian Volkert, and Ström-Olsen[11] found that the resistivity did not change appreciably with grain size, indicating that the relatively high resistance is intrinsic to the O_h^7 crystal structure, and not a result of the fine-grained microstructure.

Because classical nucleation and growth models assume the existence of only two phases, we expect this type of analysis can only be applied to the formation of the transient phase itself (at high temperatures and early times, when the bct volume fraction is still small) or at relatively low temperatures, where the fcc volume fraction never exceeds a few percent. Both analyses will be discussed.

Based on microscopic measurements of particle sizes in $NiZr_2$ and related zirconium glasses, Blank-Bewersdorff and Köster[14] have shown that the dimensions of crystallites grow linearly with time. In terms of the linear growth rate γ, the volume fraction as a function of time may be represented by

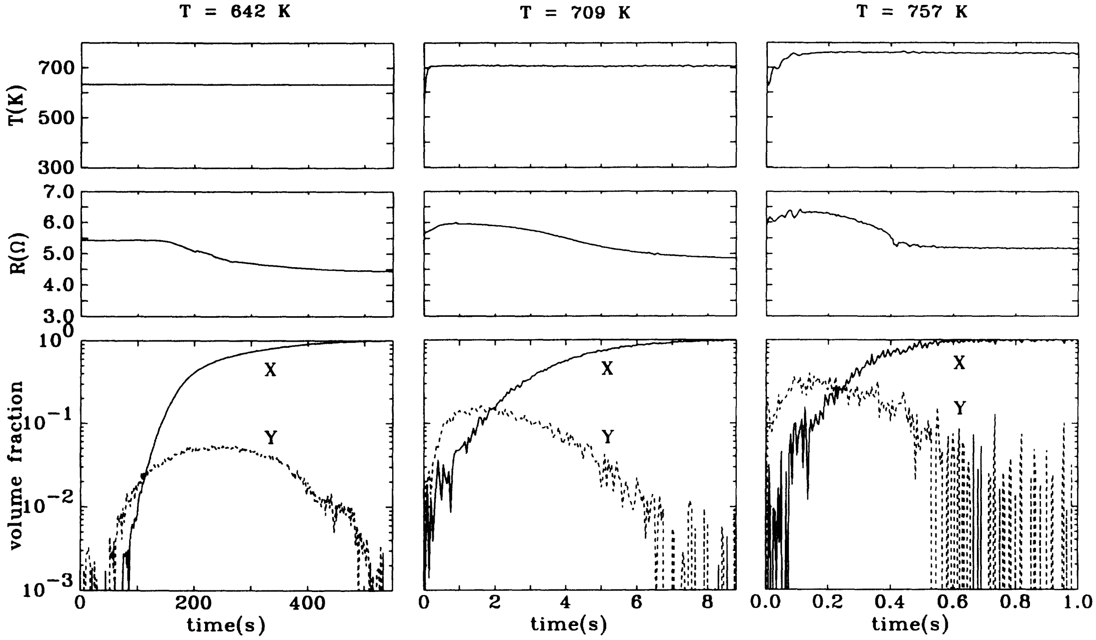

FIG. 4. Sample temperature (T), resistance (R) and volume fractions of bct (X) and fcc (Y) phases for $T=642$, 709 K, and 757 K.

$$-\ln(1-X)=\gamma^3\int_0^t I(t')(t-t')^3 dt' , \qquad (3)$$

when account is made for interparticle impingement.[15] $I(t)$ is the time-dependent nucleation rate given by an approximate theory of nucleation as

$$I(t)=I_0\left[1+2\sum_{m=1}^{\infty}(-1)^m\exp(-m^2t/\tau)\right] , \qquad (4)$$

where τ is the incubation or induction time, and I_0 is the steady-state nucleation rate. Figure 5 shows how well such a simple model works for predicting the total crystallized volume fraction at $T=642$ K. We have identified the problem of deviations of the fit for volume fractions above $X=40\%$ as resulting from larger than expected temperature gradient across the sample width. As this affects the evolution of all phases nearly equally and is approximately constant for all transformation temperatures, the analysis presented here is not affected. This effect is planned to be addressed in a subsequent publication. Although a transient in the nucleation is clear, the fit does not constitute a stringent test of transient nucleation theory, since steady-state nucleation is reached by the time there is a measurable volume fraction. As discussed in detail later, the transient may result from the formation of the fcc phase as a precursor to the bct phase.

The steady-state nucleation rate is predicted by Becker and Döring,[16] and later by Langer[17] to vary exponentially in inverse temperature. For the three lowest temperatures, 628, 635, and 642 K, the temperature dependences of τ and $\gamma^3 I_0$ are consistent with such Arrhenius behavior. The activation energy of 3 eV is in agreement with calorimetric data.

A summary of the time resolved x-ray data is shown in the form of a time-temperature-transformation diagram in Fig. 6. The square points refer to the fcc phase. The solid points are the results of fitting the data with the model of Eq. (2) and the hollow points were obtained from the onset of fcc peak intensities as determined by visual inspection. The agreement between these two methods is apparent, although points obtained via fitting have a significantly smaller scatter. The data follow an Arrhenius form suggesting that the kinetics are dominat-

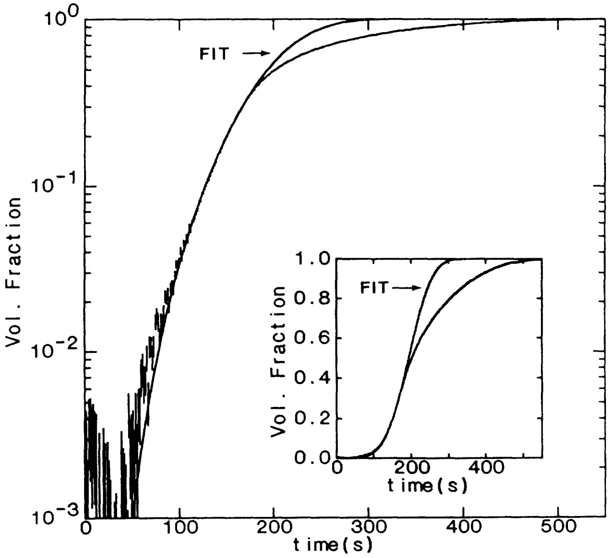

FIG. 5. The time dependence of the crystalline volume fraction for $T=642$ K. The solid curve is a fit by Eq. (3) as discussed in the text, with $\tau=13.1$ s and $\gamma^3 I_0=3.9\times10^{-7}$ s^{-4}. The error bars shown indicate the uncertainty resulting from the nonlinear least-squares fitting technique. Inset: the volume fraction on a linear scale. For times longer than 150 s, only every fifth data point is shown.

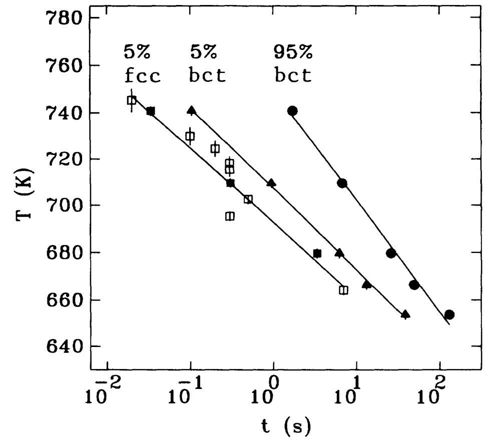

FIG. 6. Time-temperature-transformation diagram for crystallization of $NiZr_2$. The solid points are results obtained from fitting the *in situ* data with the model (2), while the hollow points are from the onset of fcc peak intensities as determined by visual inspection. The 5% transformed lines have a slope corresponding to an activation energy of 3.0±0.2 eV and 2.7±0.2 eV for the fcc and bct phases respectively. The 95% bct line gives and activation energy of 2.0±0.2 eV, suggesting that the growth process has a lower activation energy than the nucleation.

ed by the temperature dependence of mobility. All measurements were taken at temperatures well below that where the crystallization rate reaches a maximum, so, it is reasonable to expect that the transformation be controlled by the kinetics of atomic motion rather than thermodynamic driving force. The data for 5% fcc and 5% bct show nearly the same slope. The higher slope of the 95% bct data suggests that the activation energy for the growth of the bct phase is somewhat smaller than the energy barrier for nucleating that phase.

B. Characterization of quenched samples

Post-crystallization x-ray diffraction and transmission electron microscopy (TEM) studies[18] were conducted. Figure 7 shows an electron micrograph and associated diffraction pattern of the initial amorphous state. The material is homogeneous with broad diffraction halos.

Typical crystallites of the bct phase, formed at 722 K, are shown in Figs. 8(a) and 8(b). They are distributed uniformly through the bulk, with random orientations and have a mean diameter of $\approx 0.1\ \mu m$. The crystallites exhibit an extremely high density of planar defects, resulting in jagged edges and streaks in the micrograph and rods in the ⟨110⟩ direction of the single-crystal diffraction pattern [Fig. 8(c)]. These defects have been previously reported by several authors and seem to occur for all crystallization temperatures, with increased density at higher temperatures. The mean separation between the faults in Fig. 8(b) is ≈15 Å as measured spatially and from the length of the diffraction rods. Feng *et al.*[19] have ascribed these defects to 120° stacking faults normal to the ⟨110⟩ direction. The high-resolution electron micrograph of Fig. 8(d) clearly shows unfaulted layers of crystal separated by stacking defect planes, which are several lattice spacings apart. The fringes *within* each layer exhibit three possible orientations, confirming the model of 120° rotational stacking faults. The three orientations are distributed randomly indicating that the interfacial energy between any pair is equal. The high density of defects indicates that the bct structure does not pack well along a ⟨110⟩ direction in this system.[19]

The microstructure of a specimen crystallized in ≈75 ms at 776±15 K and then rapidly quenched to capture the transient fcc phase is shown in Fig. 9(a). The specimen is almost 100% fcc phase. Very high nucleation rates have resulted in the formation of a large number of roughly spherical grains of diameter ≈250 Å, distributed uniformly throughout the sample. The associated selected-area electron-diffraction pattern, shows that each of the amorphous halos is replaced by a band of Scherrer rings.

X-ray diffraction was also used to determine the crystal structure. Figure 10 is a graphite-monochromated Cu K_α $\theta-2\theta$ x-ray-diffraction scan of a specimen that is ≈95% fcc $NiZr_2$. The calculated peak positions and intensities for the O_h^7 and the D_{4h}^{18} structures are indicated. By deconvolving the resolution function of the diffractometer, the root-mean-square particle size of the fcc particles was found to be 200±40 Å in agreement with the real-space microscopy and the *in situ* results. By fitting the peak positions to the fcc structure, the lattice constant was determined to be 12.61±0.01 Å. To obtain single-crystal diffraction patterns from these extremely small particles, focused beam electron diffraction was used. The ⟨211⟩ projection shown in Fig. 9(b) confirms this indexing. The lattice constant implies a packing fraction of 0.68, rather small compared with the packing fraction of the same structure in similar systems (average ≈0.79).[20] We attribute this to chemical disorder within the material; interchanging atoms of significantly different size will lower the packing fraction as a rule. Chemical disorder is a reasonable consequence of such rapid formation.

It is useful to consider the existence of the fcc phase in other (transition-metal) $-Zr_2$ systems for which the bct is the stable phase. The stability of the structure decreases as the transition metal is changed along the progression Fe-Co-Ni of the Periodic Table. Reported crystallization

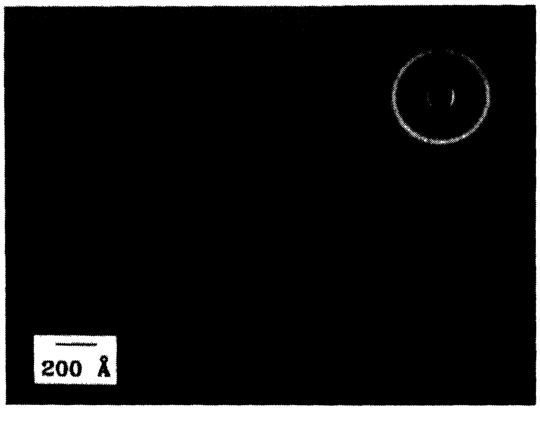

FIG. 7. Electron micrograph of amorphous $NiZr_2$ with associated diffraction pattern.

temperatures from scanning-calorimetry measurements are shown in Table I, for a row of transition metals of nearly equal size. At the heating rate of 10 Ks^{-1}, $\mathrm{FeZr_2}$ retains the fcc structure for several hundred degrees above the formation temperature, in $\mathrm{CoZr_2}$ it remains for only 50° and in $\mathrm{NiZr_2}$ it is not observed to form. The formation of $\approx 100\%$ fcc $\mathrm{NiZr_2}$ is possible however, at the limit of our most rapid *in situ* experiments. The dependence of stability on the species of transition metal suggests that the transition-metal-zirconium interaction plays a key role in determining the energy of the fcc structure.

The fcc phase has been observed in systems other than zirconium alloys. Indeed, $\mathrm{NiTi_2}$ is the prototype of the structure. In most systems it is believed to be a metastable state that can be stabilized by the presence of oxygen. The phase has been reported in $\mathrm{NiZr_2}$ containing a few percent oxygen[13,21] and was used to interpret broad weak diffraction lines in $\mathrm{CoZr_2}$.[12] (We have also studied the $\mathrm{CoZr_2}$ system and found that samples of 100% fcc phase with sharp diffraction lines corresponding to a lattice parameter of 12.28±0.02 Å could be formed during sufficiently rapid crystallization.) Several authors report the existence of an exothermic reaction in related systems (particularly slightly Ni-rich alloys), often resulting in an enhanced resistivity, but no observable crystals.[10,22] It is our belief that these observations can be attributed to very fine-grained fcc structure, and that rapid crystallization experiments would produce greater volume fractions and larger crystals of the fcc phase.

TABLE I. Crystallization temperatures for (transition-metal) -$\mathrm{Zr_2}$ glasses, from scanning-calorimetry measurements at 10 $\mathrm{K\,min^{-1}}$.

Compound	T_{fcc} (K)	T_{bct} (K)	Reference
$\mathrm{FeZr_2}$	680	1035[a]	11
$\mathrm{CoZr_2}$	705	785	12
$\mathrm{NiZr_2}$		665	8

[a] From resistivity.

Figure 11 shows the morphology of coexistence of the fcc and bct phases, for a sample partially crystallized at 720 K. The number density of particles of each phase was deduced in the following manner: volume fractions of each phase were calculated from the x-ray data, mean-particle sizes for the fcc phase were obtained from the *in*

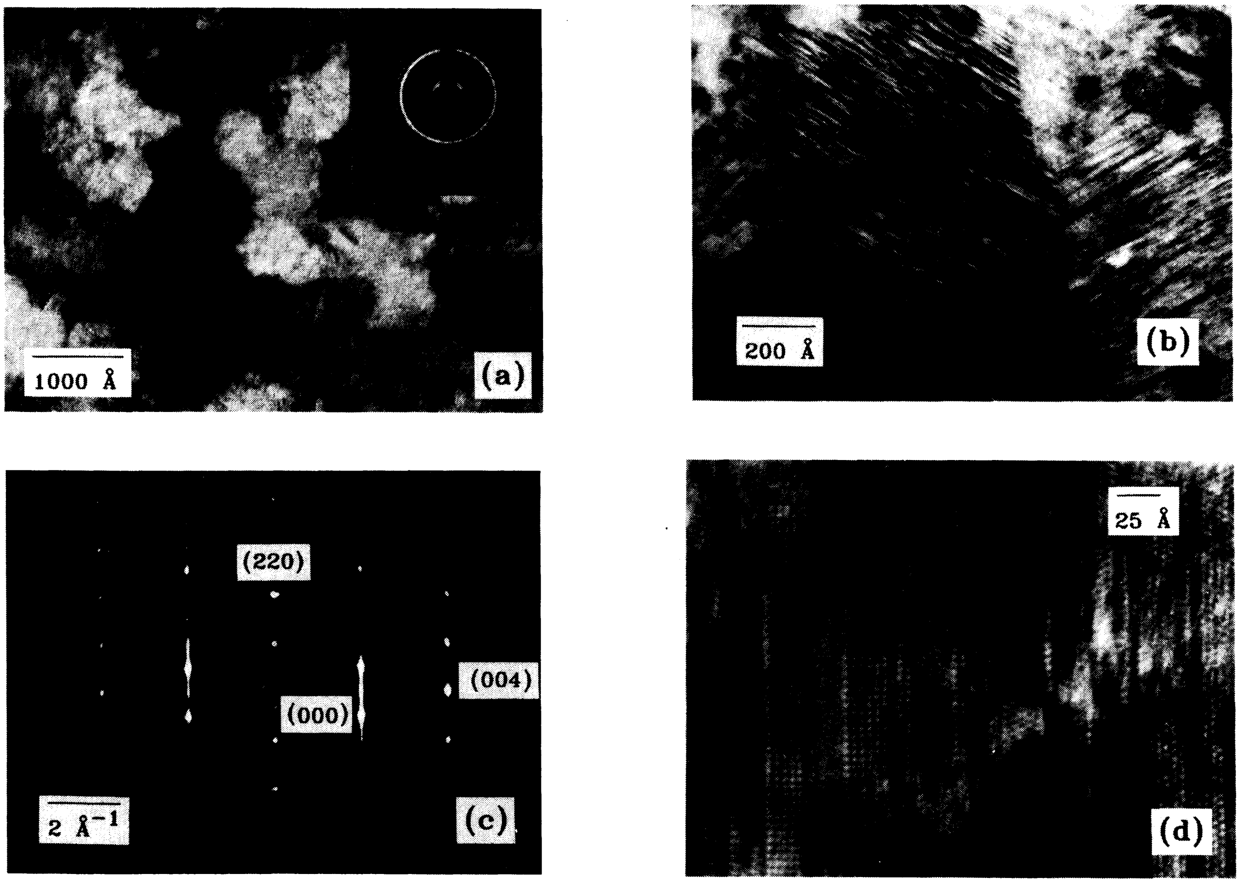

FIG. 8. Typical crystallites of bct $\mathrm{NiZr_2}$ in an amorphous background with associated diffraction pattern (a). Enlarged view of bct crystallites showing the extremely high density of planar defects (b), which give rise to rods in the ⟨110⟩ direction of the single-crystal diffraction pattern (c). A high-resolution electron microscopy image of a bct crystal (d) shows unfaulted (110) layers separated by stacking defect planes that are several lattice spacings apart. The fringes *within* each layer exhibit three possible orientations, confirming the model of 120° rotational stacking faults.[19]

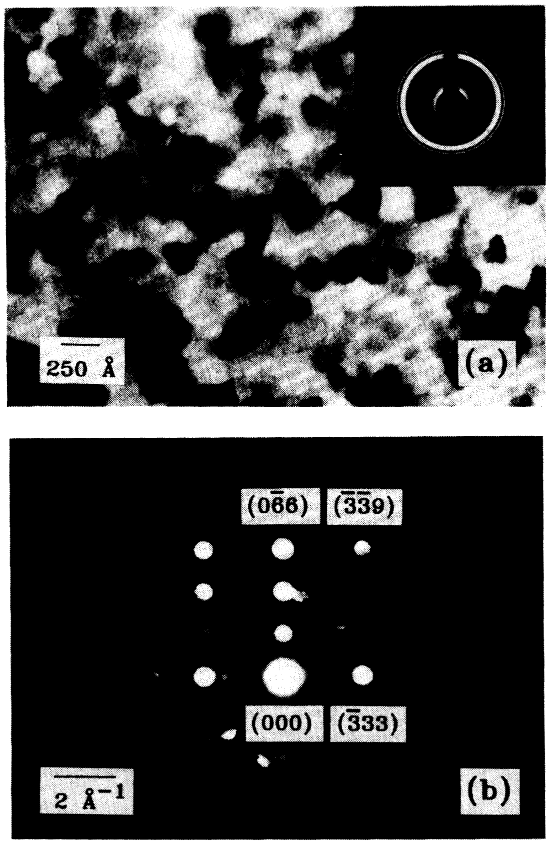

FIG. 9. (a) Microstructure and diffraction pattern of fcc $NiZr_2$ heated for ≈75 ms during one of our most rapid, but nonisothermal, crystallization experiments (776±20 K). The average grain size is ≈250 Å, the largest we have observed. Convergent beam electron diffraction (b) of one of the crystals in (a). The indexing corresponds to be the (211) projection of the O_h^7 structure with a lattice constant of 12.61±0.01 Å.

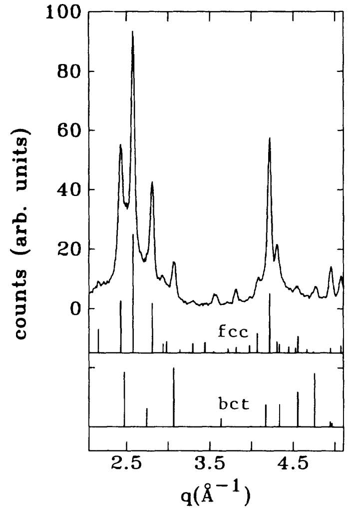

FIG. 10. Room temperature Cu $K\alpha$ x-ray-diffraction scan of $NiZr_2$ for a sample similar to that of Fig. 9. Vertical lines indicate calculated positions and relative intensities of Bragg peaks for the fcc and bct phases. The specimen is almost 100% fcc phase.

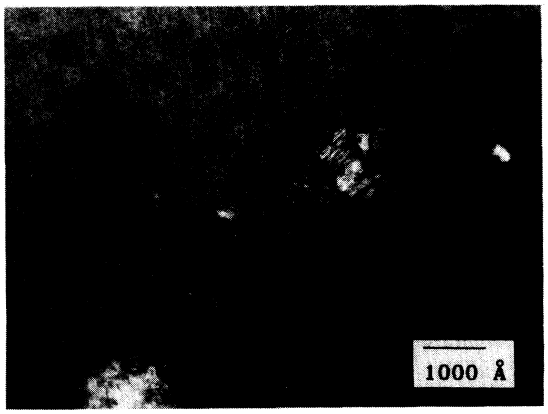

FIG. 11. The coexistence of fcc and bct $NiZr_2$ in a partially crystallized specimen. As described in the text, we deduce that there are approximately 100 fcc particles for each of the (four large) bct crystals in this micrograph, implying that the small light and dark flecks interspersed with the amorphous, a few of which are indicated with arrows, are the fcc phase.

situ scattering data by deconvolving the instrumental resolution and then using the method of Stokes and Wilson as discussed in Warren,[23] mean-particle sizes of the bct phase were measured from micrographs like Fig. 11; and the volume fraction divided by the average particle volume gives the number density of the phase. As an example, the specimen of Fig. 11 has mean-particle sizes of ≈1000 Å for the bct phase and ≈80 Å for the fcc phase. Thus the ratio of mean-particle volumes is ≈2000. The volume fractions bct and fcc are 20% and 1%, respectively so we deduce that there are ≈100 fcc particles for every bct. This implies that the small, barely visible light and dark flecks interspersed with the amorphous, are the fcc phase. At lower transformation temperatures, the fcc grains become smaller and so are not detectable by TEM.

Using the calculated particle density, we can estimate the nucleation rate for the fcc phase given the total trans-

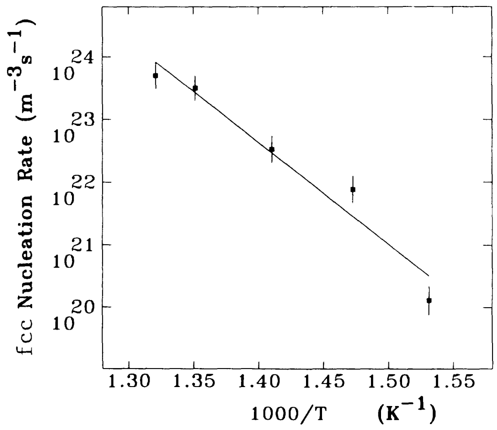

FIG. 12. Temperature dependence of nucleation rate for crystallization of fcc $NiZr_2$. The slope gives an activation energy of 3.2±0.4 eV, which is the same as the 5% transformed curves of Fig. 6.

formation time and assuming the nucleation rate to be approximately constant.[24] The results are given in Fig. 12. The activation energy for nucleation is given by the best-fit slope to be 3.2 ± 0.4 eV, and is the same as that obtained for the 5% transformation curves of both the fcc and the bct phase.

IV. DISCUSSION

At all temperatures, our *in situ* x-ray-scattering data shows the formation of small quantities of the fcc phase *before* the bct begins to form. The fcc scattering then diminishes as the bct phase grows. This suggests that the fcc phase is actually a precursor to the bct phase. One consequence of such a two-step process would be the requirement of transient nucleation of the bct phase. At low temperatures, where the bct phase is primarily formed, the Johnson-Mehl-Avrami analysis[15] of our *in situ* bct data gives Avrami exponents of $n \geq 4$ implying that the nucleation is homogeneous with rates increasing with time. Also, it has been found by the method of crystallization statistics, that nucleation of the bct phase in $CoZr_2$ and $NiZr_2$ occurs with transient rates.[14] Transient nucleation implies that some appreciable fraction of the crystallization time is required for sufficient thermodynamic fluctuations to occur for the nucleation rate to reach the steady-state value. We propose that in these systems, the incubation time may largely result from the time required to form a sufficient population of small fcc particles, which themselves nucleate homogeneously throughout the amorphous matrix. In this model, crystallites of bct phase then nucleate from the fcc and grow to fill the available volume, overtaking the fcc particles in the process. Although we cannot rule out the possibility of the bct phase nucleating independently from the amorphous in parallel with the two-step process, a serial two-step model is sufficient to explain our observations.

The maximum volume fraction of fcc phase increases with temperature. This implies that the ratio of rates of amorphous-to-fcc transformation to fcc-to-bct transformation, increases with temperature. However, from the parallel slopes of the 5% transformed lines in Fig. 6, we see that the activation energies of nucleation are nearly the same for both transformations. The simplest explanation is that the nucleation of fcc phase controls the nucleation of the bct phase, and that the bct phase has a lower activation energy for growth. This also explains why the 95% bct curve of Fig. 6 is of higher slope.

The mean width of the fcc peaks was observed to *decrease* with higher anneal temperature, and thus faster kinetics. A larger volume fraction of fcc material forms at higher temperatures because the fcc phase forms more rapidly with respect to the bct phase. Hence, larger crystals are expected at higher temperatures, since fcc growth is governed by approximately the same activation energy as nucleation of that phase. It is important to note that, in all of our isothermal data, growth of the fcc particles is not limited by impingement because the fcc particles are overtaken by the bct phase.

It appears that the *d*-band electronic structure plays a key role in determining the relative stabilities of the two-crystal phases. Susceptibility measurements[25] and ultraviolet photoemission spectroscopy[26] show diminished density of states at the Fermi surface along the progression from Fe-Co-Ni-Cu in (transition-metal) -Zr_2 glasses. This is because the *d* band arising from the transition-metal 3*d* shell, sits further below the Fermi surface as the 3*d* shell becomes more filled. As mentioned previously, in the progression from Fe-Co-Ni, the fcc phase is a decreasingly favorable step *en route* to the bct phase. The trend suggests that the energy barrier for transformation from the fcc to the bct structure decreases along the progression. The simplest explanation is that the relative stability of the fcc phase is reduced with the closing of the transition-metal 3*d* shell.

We believe that the crystallization proceeds in two steps because the fcc phase is structurally closer to the amorphous than the bct. The fcc structure is more complex, with nominally 24 atoms in the primitive unit cell, as compared to the six-atom bct cell. Moreover, the cubic structure retains more of the structural symmetries of the amorphous phase than does the tetragonal. Figure 13 shows the pair-pair correlation functions for amorphous $Ni_{35}Zr_{65}$ as measured by Lee *et al.*[27] The interatomic distances and partial coordination numbers deduced from this data are the same as those reported more recently by Paul and Frahm[28] in $NiZr_2$. Also shown are coordination shells for both the fcc and bct structures. The Zr-Zr and in particular the Ni-Zr shells of the fcc are more similar to the amorphous than those of the bct. The Zr-Zr coordination is more important than the Ni-Ni coordination because of topology; Zr atoms are $\approx 30\%$ bigger than Ni atoms. The importance of unlike neighbor interactions is clear from the sensitivity of the structural stability on the type of transition metal and the large heat of mixing for Ni and Zr.[29] The relative similarity between the fcc coordination shells and the amorphous pair-pair correlation functions suggests that the fcc structure requires less energy to rearrange from the amorphous matrix. We believe this to be the reason why the fcc phase has a much higher nucleation rate than the bct at a given temperature.

We have considered the possibility that impurity diffusion plays a role in the crystallization kinetics. The stability of the fcc phase is strongly affected by oxygen content.[13] The fcc phase can easily accommodate the ≈ 0.2 at. % oxygen impurities introduced when the samples are made. If the solubility of oxygen in bct $NiZr_2$ is less than 0.2%, the bct growth may be limited by the diffusion of oxygen out of developing crystallites. However, this solubility threshold is exceedingly low. Moreover, the oxide that would result from such a process [$Zr_{67}Ni_{22}O_{11}$ (Ref. 30)] is quite oxygen deficient, so that 0.2% oxygen would form ≈ 1.5 vol % oxide phase. We see no evidence for this phase in our x-ray scattering or microscopy data. It seems that the oxygen impurities stay in solution in the bct phase.

We mention in closing that in some of our most rapid crystallization experiments in $NiZr_2$ and $CoZr_2$, other transient phases have been observed. Although the transformation was so rapid that temperature uniformity was not maintained throughout the transformation, clear

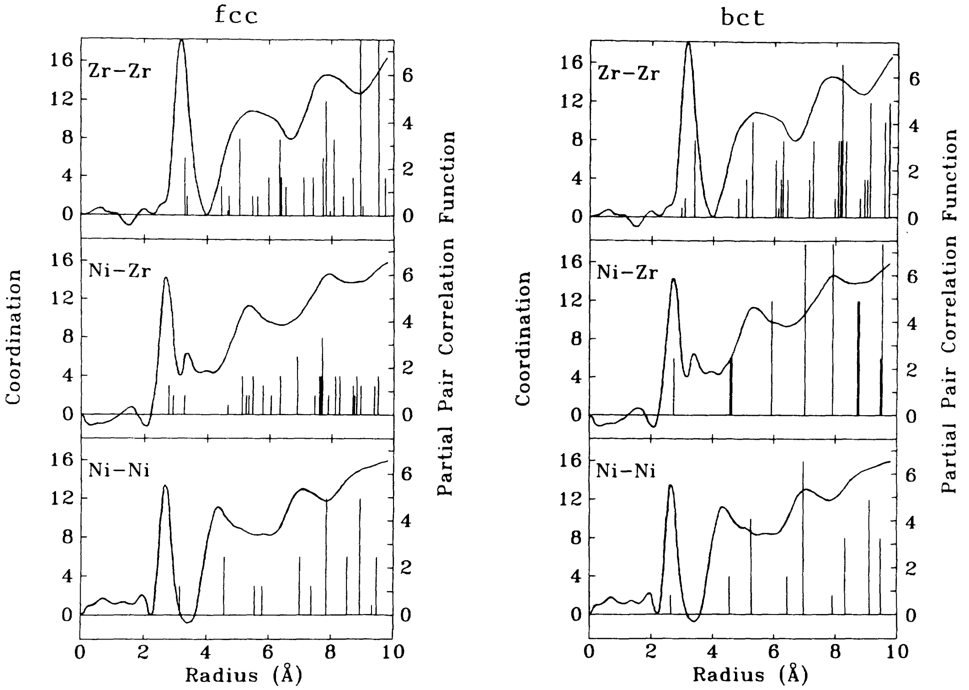

FIG. 13. Pair-pair correlation functions for amorphous $Ni_{35}Zr_{65}$ taken from[27] are shown as smooth curves. The superimposed histograms indicate the number of neighboring atoms as a function of radius (coordination) for the fcc and bct structures, respectively. Compared to the bct, the coordination shells of the fcc structure are more similar to the amorphous for Zr-Zr and, particularly, Ni-Zr neighbors. As discussed in the text, these two correlations have the strongest effect on the energy to convert one structure to another. We believe that the higher nucleation rates observed for the fcc phase, compared to the bct, reflect the structural similarity between the amorphous and the fcc phase.

diffraction peaks of an as yet unidentified structure were observed for about 10 ms before the formation of fcc $NiZr_2$ at ≈ 850 K. In $CoZr_2$, an unidentified phase appears after the fcc phase and before the bct, during rapid transformations.[31]

We have seen that a simple transient nucleation model can be applied to the crystallization process in $NiZr_2$ at sufficiently low temperatures and thus slow kinetics; as the equilibrium rate is increased, transformation proceeds in two steps. At still higher equilibration rates, it seems that the system can sample yet more configurations on its way to the lowest-energy structure. A reevaluation of classical theories is needed to explain nucleation and growth in these systems, since existing theories assume the coexistence of only the initial and final phases.

ACKNOWLEDGMENTS

We sincerely thank Zaven Altounian for many fruitful discussions. We also acknowledge the efforts of Jean Jordan-Sweet, Karl Ludwig, Jr., and Jacques Mainville, who participated in the early time-resolved scattering experiments. This work was supported in part by the Natural Sciences and Engineering Research Council of Canada and les Fonds pour la Formation des Chercheurs et l'Aide à la Recherche de la Province du Québec. The MIT part of the IBM-MIT consortium is supported by the National Science Foundation, Materials Research Laboratory Program under Grant No. DMR84/18718. The National Synchrotron Light Source is supported by the U.S. Department of Energy, Division of Materials Sciences and Division of Chemical Sciences (DOE Contract No. DE-AC02-76CH00016).

APPENDIX: FITTING FUNCTIONS FOR SCATTERING PATTERNS

Generally, the best functions to use for determining the volume fraction of the initial and final phases in a two-phase transformation, are the initial and final scattering data. If intermediate scattering patterns are well described by a linear combination of these two, the coefficients of linear combination give the volume fraction directly. Since the integrated scattering intensity of one phase is proportional to the volume of material giving rise to that phase, and, since the shape of the scattering from each phase does not change, the integrated intensity is proportional to the intensity itself.

However, if there are more than two phases present, the intermediate scattering patterns will not be well described by a combination of the first and the last. The same is true for transformations where the shape of scattering from one or more phases changes during the transformation. This may occur for example if particles, which are smaller than the resolution limit grow, or if the lattice constant changes, during the transformation. To determine volume fractions in such cases we require an analytical model for the scattering of each phase. In principle, the peak positions and intensities for a given crystal structure can be calculated. In practice, it is easier to construct a simple model for the scattering, and fit the scattering pattern with the model to establish the best parameters. In our analysis, the model parameters are obtained from a prefit to the initial and final diffraction patterns. Then, by fitting intermediate patterns as a linear combination and varying one or more shape parameters, we can extract volume fraction as well as additional structural information about the phases as a function of time.[32] Prefitting has the additional advantage of averaging intensity fluctuations caused by limited counting statistics.

The prefitting function used to describe the scattering I_X of a crystalline phase is the sum of Bragg peaks; thus,

$$I_X(q)=\sum_i a_i p_i(q) , \tag{A1}$$

where a_i is the area of peak *i*. The peak shape function p_i is a sum of Gaussian and Lorentzian line shapes having equal widths at half maximum, w_i. Explicitly,

$$\begin{aligned} p_i(q)=&(1-f_i)\frac{1}{\pi w_i}\frac{1}{[1+(q-q_i^0/w_i)^2]} \\ &+f_i\left[\frac{\ln 2}{\pi w_i^2}\right]^{1/2}\exp[\ln 2(q-q_i^0/w_i)^2] , \end{aligned} \tag{A2}$$

where $f_i \in (0,1)$ is the Gaussian fraction. Both the Gaussian and Lorentzian terms in the peak shape function have unit area, as does p_i. The peak positions, q_i^0, are calculated from the lattice parameters and the indices of the Bragg peaks.

We have found this peak shape function to effectively parametrize the observed Bragg peaks. Often a Gaussian fraction of $f_i=1$ provides a good fit to our observed line shape. Sometimes however we observe extra scattering in the tails, most likely due to stacking faults and other defects. By decreasing the Gaussian fraction, the tails are enhanced at the expense of the central portion of the peak so that the area under the peak conserved. Also, the normalization ensures that changing the width leaves the area under the peak unchanged. Conservation of peak area is important, since the volume fraction is proportional to the integrated area.

To account for thermal diffuse and isotropic gas scattering, a linear background of the form $b_i q + c_i$ is often added to the sum of Eq. (A1). The scattering pattern of the amorphous phase is often well fit by a broad Gaussian peak on a linear background.

For experiments where the lattice parameters change during the transformation due to temperature or composition changes, the lattice parameters can be multiplied by a common factor to fit the peak positions. Similarly, the widths can be multiplied by a factor to account for sharpening during the transformation. Of course, we always vary the least number of fit parameters required to explain the data. In $NiZr_2$, I_{bct} (and I_{fcc}) were held constant. It should be noted that the prefitting model can be easily extended to account for stacking faults, disordering etc., within the framework of the kinematic theory of x-ray scattering.

---

[1] U. Köster, U. Schünemann, G. B. Stephenson, S. Brauer, M. Sutton, in *Materials Research Society Symposia Proceedings: Kinetics of Phase Transformations, Fall Meeting, 1990,* edited by M. O. Thompson, M. J. Aziz, G. B. Stephenson, and D. Cherns (North-Holland, Amsterdam, 1990).

[2] M. Sutton, Y. S. Yang, J. Mainville, J. L. Jordan-Sweet, K. F. Ludwig, Jr., and G. B. Stephenson, Phys. Rev. Lett. **62**, 288 (1989).

[3] S. Brauer, D. H. Ryan, J. O. Ström-Olsen, M. Sutton, and G. B. Stephenson, Rev. Sci. Instrum. **61**, 2214 (1990).

[4] G. B. Stephenson, K. F. Ludwig, Jr., J. L. Jordan-Sweet, S. Brauer, J. Mainville, Y. S. Yang, and M. Sutton, Rev. Sci. Instrum. **60**, 1537 (1989).

[5] Optical multichannel analyzer (Model 1412 detector, Model 1461 controller), EG&G Princeton Applied Research, P.O. Box 2565, Princeton, NJ 08540.

[6] M. Sutton, Y. S. Yang, J. Mainville, J. O. Ström-Olsen, Z. Altounian, G. B. Stephenson, and K. F. Ludwig, Jr., Mater. Sci. Eng. **97**, 307 (1988).

[7] Model MR-6015-06C, IRCON Inc., Niles, IL 60648.

[8] Z. Altounian, Guo-Hua Tu, and J. O. Ström-Olsen, J. Appl. Phys. **54**, 3111 (1983).

[9] M. E. Kirkpatrick, D. M. Bailey, and J. F. Smith, Acta Crystallogr. **15**, 252 (1962).

[10] R. Schulz, V. Matijasevic, and W. L. Johnson, Phys. Rev. B **30**, 6856 (1984).

[11] Z. Altounian, C. A. Volkert, and J. O. Ström-Olsen, J. Appl. Phys. **57**, 1777 (1985).

[12] Z. Altounian, R. J. Shank, and J. O. Ström-Olsen, J. Appl. Phys. **58**, 1192 (1985).

[13] Z. Altounian, E. Battalla, J. O. Ström-Olsen, and J. L. Walter, J. Appl. Phys. **61**, 149 (1987).

[14] M. Blank-Bewersdorff and U. Köster, Mater. Sci. Eng. **97**, 313 (1988).

[15] J. W. Christian, *Transformations in Metals and Alloys,* 2nd ed. (Pergmamon, New York, 1975), Pt. 1.

[16] R. Becker and W. Döring, Ann. Phys. (Leipzig) **24**, 719 (1935).

[17] J. S. Langer, Ann. Phys. (New York) **54**, 258 (1969).

[18] Phillips CM20 operating at 200 kV. Samples were prepared by electrochemical thinning in methanol plus 5% perchloric acid at −20 °C.

[19] Y. C. Feng, K. H. Kuo, Z. K. Hei, and Y. K. Wu, Philos. Mag. A **56**, 757 (1987).

[20] J. D. H. Donnay and H. M. Ondik, *Crystal Data Determinative Tables,* 3rd. ed. (U.S. Department of Commerce, National Bureau of Standards and the Joint Committee on Powder Diffraction Standards, Swarthmore, PA, 1983).

[21] R. Brüning, Z. Altounian, J. O. Ström-Olsen, and L. Schultz, Mater. Sci. Eng. **97**, 317 (1988).

[22] K. H. J. Buschow, B. H. Verbeek, and A. G. Dirks, J. Phys. D **14**, 1087 (1981).

[23] B. E. Warren, *X-ray Diffraction* (Addison-Wesley, Reading, MA, 1969).

[24] We have used the integral breadth method outlined by Warren (Ref. 23). The integral breadth in **q** space β is the ratio of peak area to peak height. With the assumption of spherical

particles, which both nucleate and grow at uniform rates without impingement, it can be shown that the nucleation rate per unit volume is $I \approx 5\times10^{-4}\beta^3 x/t$, where x is the volume fraction of crystals measured at time t.

[25] Z. Altounian and J. O. Ström-Olsen, Phys. Rev. B **27**, 4149 (1983).

[26] P. Oelhafen, in *Glassy Metals II*, edited by H. Beck and H.-J. Güntherodt (Springer-Verlag, New York, 1983), Chap. 9.

[27] A. E. Lee, S. Jost, C. N. J. Wagner, and L. E. Tanner, J. Phys. (Paris) Colloq. **48**, C8-181 (1985).

[28] F. Paul and R. Frahm, Phys. Rev. B **42**, 10 945 (1990).

[29] G. C. Wong, W. L. Johnson, and E. J. Cotts, J. Mater. Res. **5**, 488 (1990).

[30] M. V. Nevitt and J. W. Downey, Trans. Metall. Soc. AIME **221**, 1014 (1961).

[31] Y. S. Yang, Ph.D. thesis, McGill University, 1989.

[32] U. Köster, U. Schünemann, M. Blank-Bewersdorff, S. Brauer, M. Sutton, G. B. Stephenson, in Proceedings of the 7th International Conference on Rapidly Quenched Metals, Stockholm, (1990) [Mater. Sci. Eng. **A113**, 611 (1991)].

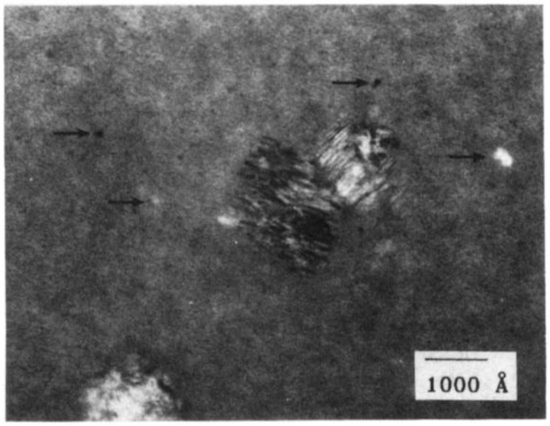

FIG. 11. The coexistence of fcc and bct $NiZr_2$ in a partially crystallized specimen. As described in the text, we deduce that there are approximately 100 fcc particles for each of the (four large) bct crystals in this micrograph, implying that the small light and dark flecks interspersed with the amorphous, a few of which are indicated with arrows, are the fcc phase.

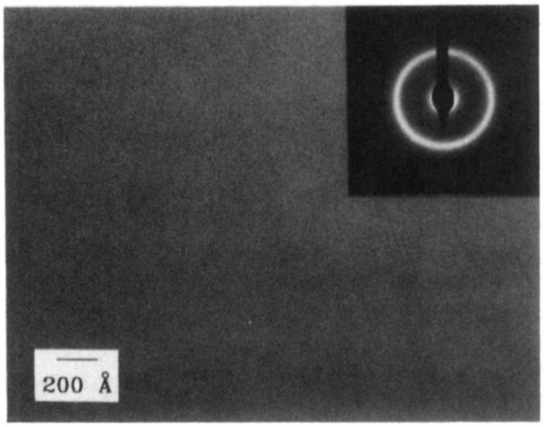

FIG. 7. Electron micrograph of amorphous $NiZr_2$ with associated diffraction pattern.

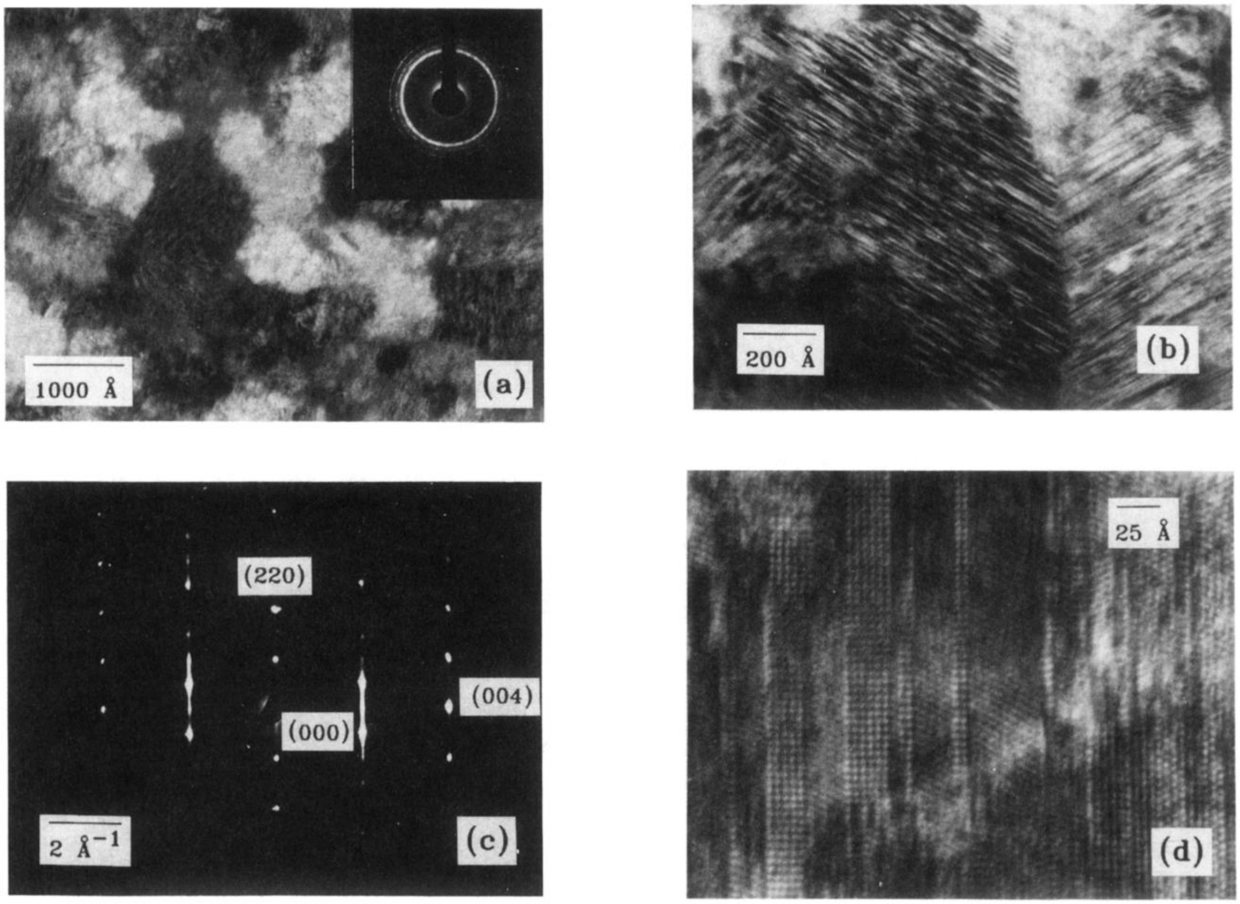

FIG. 8. Typical crystallites of bct NiZr$_2$ in an amorphous background with associated diffraction pattern (a). Enlarged view of bct crystallites showing the extremely high density of planar defects (b), which give rise to rods in the $\langle 110 \rangle$ direction of the single-crystal diffraction pattern (c). A high-resolution electron microscopy image of a bct crystal (d) shows unfaulted (110) layers separated by stacking defect planes that are several lattice spacings apart. The fringes *within* each layer exhibit three possible orientations, confirming the model of 120° rotational stacking faults.[19]

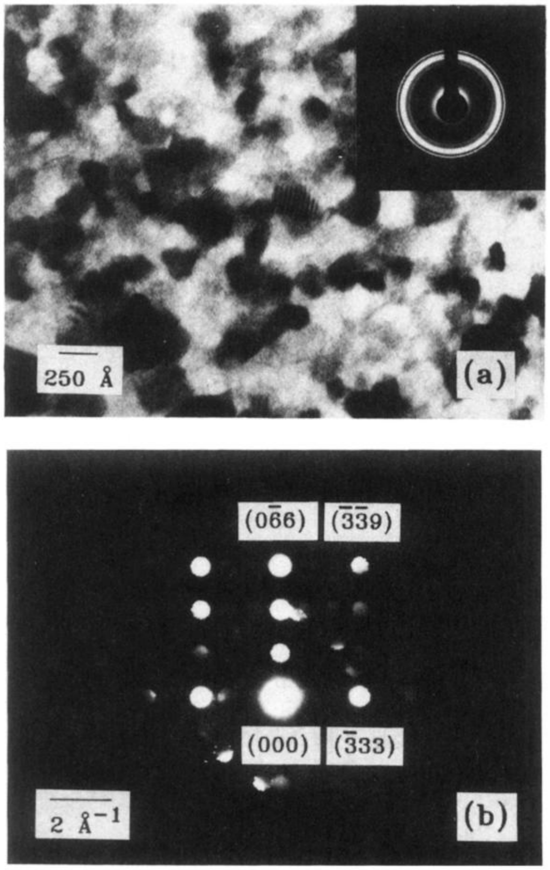

FIG. 9. (a) Microstructure and diffraction pattern of fcc $NiZr_2$ heated for ≈75 ms during one of our most rapid, but nonisothermal, crystallization experiments (776±20 K). The average grain size is ≈250 Å, the largest we have observed. Convergent beam electron diffraction (b) of one of the crystals in (a). The indexing corresponds to be the (211) projection of the O_h^7 structure with a lattice constant of 12.61±0.01 Å.